RI 9448

REPORT OF INVESTIGATIONS/1993

Seismicity and Stress Changes Subsequent to Destress Blasting at the Galena Mine and Implications for Stress Control Strategies

By F. M. Boler and P. L. Swanson

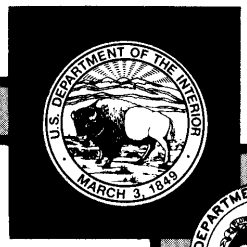

UNITED STATES DEPARTMENT OF THE INTERIOR

BUREAU OF MINES

Report of Investigations 9448

Seismicity and Stress Changes Subsequent to Destress Blasting at the Galena Mine and Implications for Stress Control Strategies

By F. M. Boler and P. L. Swanson

UNITED STATES DEPARTMENT OF THE INTERIOR
Bruce Babbitt, Secretary

BUREAU OF MINES

CONTENTS

ILLUSTRATIONS

ILLUSTRATIONS—Continued

TABLE

UNIT OF MEASURE ABBREVIATIONS USED IN THIS REPORT

ft	foot	kPa	kilopascal
h	hour	m	meter
Hz	hertz	m^3	cubic meter
J	joule	min	minute
kg	kilogram	mm	millimeter
kg/m^3	kilogram per cubic meter	MPa	megapascal
kHz	kilohertz	μs	microsecond
km	kilometer	psi	pound (force) per square inch
km/s	kilometer per second	V/g	volt per acceleration of gravity

SEISMICITY AND STRESS CHANGES SUBSEQUENT TO DESTRESS BLASTING AT THE GALENA MINE AND IMPLICATIONS FOR STRESS CONTROL STRATEGIES

By F. M. Boler[1] and P. L. Swanson[1]

ABSTRACT

The U.S. Bureau of Mines conducts research at the Galena Mine, Wallace, ID, with the aim of mitigating the effects of rock bursting. Destress blasting is commonly used as a stress control technique at the mine. A digital seismic array and an array of borehole pressure cells (BPC's) had been installed near the site of a stope undergoing mining and periodic destressing. The instrumentation was being monitored at the time of a destress blast of the 46-99 stope. No significant seismic events occurred coincident with the destress. However, the destress was followed by a 2½-week period of increased seismic activity, including two damaging events on February 7, 1990, at 034500 (hour, minute, and second) and 122020 Pacific standard time. BPC measurements indicated coseismic ground pressure changes on the order of 200 to 300 kPa associated with the damaging events. Fault plane solutions and dislocation models established that stress changes induced by the event at 034500 may have been significant in promoting the occurrence of the event at 122020. Theoretical investigations suggest that applying knowledge of the existing stress field, an understanding of rock burst mechanics, and fracture mechanics principles can improve destress effectiveness.

[1]Geophysicist, Denver Research Center, U.S. Bureau of Mines, Denver, CO.

INTRODUCTION

The U.S. Bureau of Mines conducts rock burst research in the Coeur d'Alene silver district of northern Idaho. Some of the Bureau's research effort has focused on methods of destressing burst-prone pillars (*1*).[2] As part of its program to improve safety in mines, the Bureau conducted research to show how quantitative evaluation of the effectiveness of a destress is possible.

The purpose of destressing is to eliminate or, at a minimum, reduce the rock burst danger to miners. The ultimate test of the success of a destress is whether damaging events do or do not occur once work resumes in the stope after a destress. If no damaging events occur for an extended (but unspecified) time period once work resumes, then the miners have been protected.

It is not currently possible to guarantee that a destress will achieve the desired objective, nor is it possible to tell whether the destress has achieved the desired objective until a sufficient time has passed without a damaging event. It would be desirable to (1) have a quantitative means to evaluate the effectiveness of a destress blast before work resumes in the stope, and (2) be able to tailor the design of a particular destress to the site characteristics to maximize its effectiveness.

The results of the research of the early 1970's by Blake (*1*) showed that pillar destressing by means of blasting could be helpful in controlling rock bursts. There are two ways that destress blasting may achieve the desired objective. First, the stiffness of the pillar might be reduced by fracturing caused by the blast. As in laboratory rock sample testing with a stiff loading machine, when the stiffness of the pillar (rock sample) is lower than the surrounding rock (loading machine), then unstable failure of the pillar (rock sample) is impossible. Leighton (*2*) pointed out that stresses previously borne by the pillar may be increased to dangerous levels in the surrounding rock mass by the pillar destressing. Thus, while the pillar itself might not fail unstably, some part of the surrounding rock mass might.

Second, the dynamic nature of the destress, in combination with the fracturing generated, might trigger a large seismic event that effectively releases strain energy that might otherwise be released in a rock burst. Cook (*3*) suggested that the destress could be viewed as a success only if destressing released seismic energy in excess of the energy contained in the blast itself. This is the criterion used in practice by mine management to judge destressing effectiveness at the time of the blast.

Since these early studies, destressing has been undertaken frequently at the Galena silver-lead-zinc mine, in Wallace, ID, the site of the present study, as well as other mines worldwide. The mining method at the Galena Mine is overhand cut and fill of the near-vertical silver-bearing veins. The general progression on a vein is from the surface downward, but individual stopes are mined upward between horizontal access drifts separated by a vertical distance of 90 m.

Destress blasting is typically used when two conditions occur simultaneously: (1) the overhand pillar size reaches a critical height of 10 to 20 m (*1*); and (2) an increase in numbers and rates of microseismic events detected with an accelerometer array surrounding the stope occurs. The second condition alone may be sufficient for a destress to be made.

On February 2, 1990, the 21-m-high pillar in the 46-99 stope of the Galena Mine was destress blasted. This was the second attempt at destressing this stope in 2 months; a previous attempt took place in December 1989. A subsequent destress was attempted in June 1990. No "significant" seismic event was observed coincident with any of the three destressing attempts. From the point of view of success of destressing, the size of a "significant seismic event" has been determined through experience by mine personnel. [In this report, "significant seismic event" refers to an event that generates displacements sufficient to peg the surface seismometer recording system (an event with an approximate local Richter magnitude greater than 0.7).] While no significant events coincided with the February 2 destress, several significant events occurred over the following week. Also, when mining resumed with a production blast on February 19, a significant event that caused damage in the raise followed blasting by less than 30 min. Figure 1 shows the significant events in the 46-99 stope from the period January 1989 through October 1990. The intensity of activity following the destress of February 2, 1990, is noteworthy.

Because significant events that potentially endangered miners occurred after work had resumed in the stope, the destress cannot be viewed as successful. By applying techniques to quantitatively evaluate the state of stress before and after a destress, it may be possible to identify such hazardous situations.

The significant events that followed the destress were recorded by a surface seismometer and, in most cases, by an underground digitally recorded accelerometer array. Stress-change-monitoring equipment was deployed in the vicinity of the stope and was monitored during destressing and during the following weeks.

[2]Italic numbers in parentheses refer to items in the list of references at the end of this report.

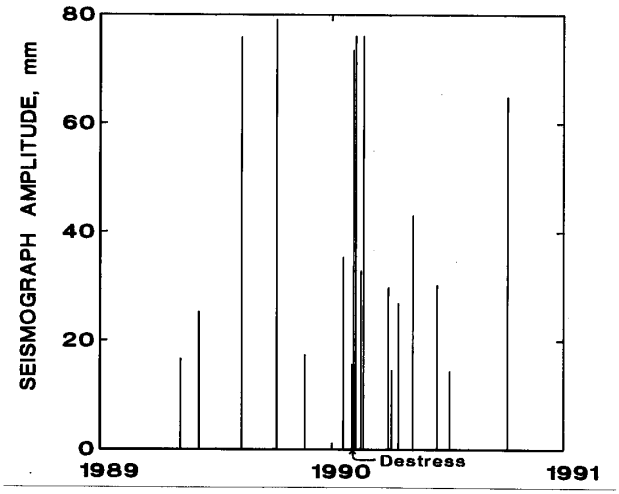

Figure 1.—Seismic activity in vicinity of 46-99 stope during January 1989 through October 1990. Number of large amplitude events in 20 days after February 2, 1990, destress represents unusual concentration of such events.

The purpose of this report is to show how quantitative evaluation of the effectiveness of a destress is possible. This is accomplished through monitoring the stress state and changing stress conditions using full waveform microseismic data as well as quasi-static rock-mechanics data. Through seismic and stress observations and subsequent modeling, the degree of stress interaction between the seismic events following the destress is examined. Digitally recorded accelerometer waveforms are used to constrain the focal mechanisms for the damaging events and several associated microseismic events. These mechanisms, along with the event locations, are used to define fault planes on which dislocation slip, constrained by stress-change measurements, is determined. These analyses show how processes surrounding destressing can be quantitatively described. With further observations, including knowledge of the near and far-field stresses, quantitative evaluation of destress effectiveness is possible. Further, knowledge of the state of stress in the area to be destressed, along with the mine and host rock structure, including fractures and faults, can lead to the design of better destress methods.

BACKGROUND

GEOLOGIC SETTING

Hobbs (*4*) discusses the geology of the district. Figure 2 shows a location map with faults in the vicinity of the Galena Mine. The country rock consists of Precambrian Belt Series quartzites and minor argillites. Much of the faulting displacement postdates mineralization. Figure 3 shows the mapped vein geology in the vicinity of the 46-99 sill drift. The vein is near vertical and strikes approximately N. 45° E. Vein offsets are indicative of postmineralization faulting; bedding plane faults striking approximately N. 45° W., cutting the vein at nearly 90°, are most common. The apparent sense of offset is typically right lateral; the maximum apparent offset (plan view) for faults in the 46-99 stope area is approximately 4 m.

LOCUS OF MAJOR SEISMIC ACTIVITY WITHIN MINE

The relationship between the locations of stopes experiencing rock bursting and the major fault trends in the immediate vicinity of the Galena Mine was recently investigated (*5*). Seismic data recorded on the surface seismograph over a 20-month observation period were correlated with rock bursts and other large seismic events that were located using dense arrays of accelerometers. Seventy percent of the stoping areas associated with the 29 largest seismic events [local magnitude (M_L) ~ 1.8 to 2.9] were found to occur on a single, well-defined, near-vertical plane during this time interval. The plane had dimensions of 1.6 km in length and 0.4 km in height and was centered 1.5 km below surface. The strike of the plane, N. 48° W., generally paralleled several 10-km-long faults mapped on the surface (fig. 2) and identified underground. The few events that did occur away from this plane during this time period took place on another structurally significant feature, the Silver Vein (dimensions of 300 by 800 m.)

While examination of the mine's geologic maps does not reveal a single major well-defined fault surface that extended continuously throughout the entire plane of major seismic activity, there are many faults of the appropriate strike and location. Wherever a significant fault is not in the appropriate position in a stope, the maps indicate the potential to accommodate slip over the same general trend and area via a series of blocky structures with bounding surfaces of similar orientation. Such is the nature of the structure in many mines of the Coeur d'Alene district. Using relationships between inferred rupture plane dimensions and seismic magnitudes published in the mining seismology literature, Swanson (*6*) shows that slip is conceivably mobilized over this entire plane.

During one 3-month period of high seismic activity, the Galena shaft, which is intersected by the plane of large seismic activity, experienced ground control problems that shut it down for repair for several months. Fault gouge from the major near-vertical fault strand that it intersects was expelled into the shaft directly above the plane of

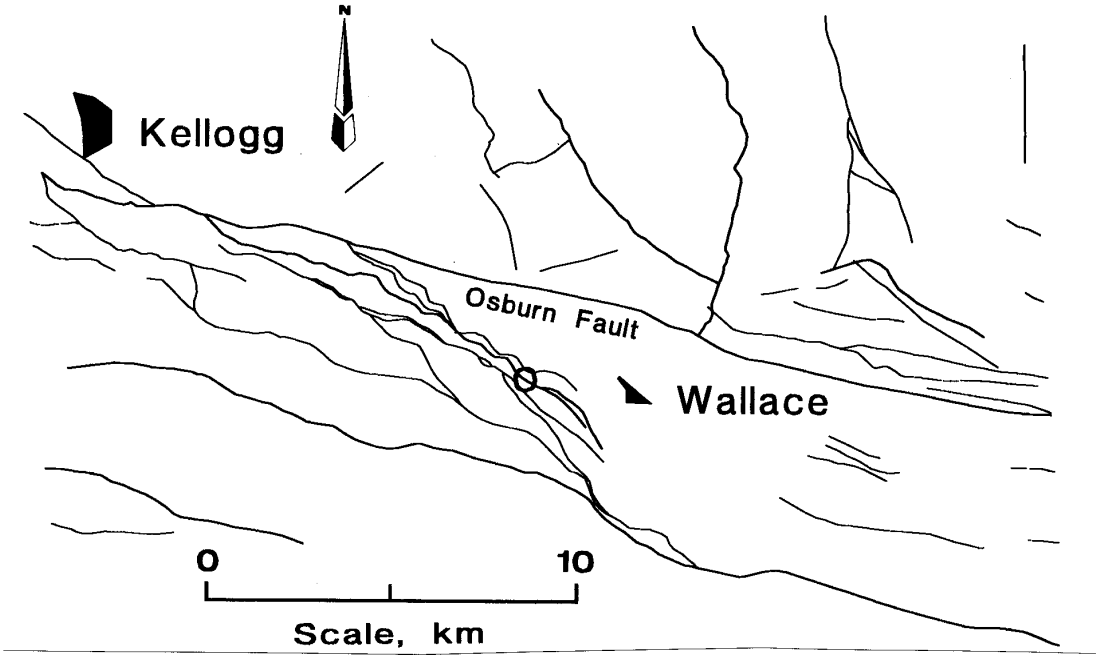

Figure 2.—Faulting in Coeur d'Alene mining district, Wallace, ID. (All lines indicate faults. Circle indicates the Galena Mine.)

seismic activity and damaged 28 timber sets. These observations suggest that the major structural discontinuities in this mine play an important role in accommodating mining-induced deformation.

DESTRESS OF FEBRUARY 2, 1990

The 46-99 stope of the Galena Mine was destressed on Friday, February 2, 1990, after the last production shift of the day. Figure 4 shows the hole pattern for the destress blast. The total amount of explosives in all the holes was 125 kg. This stope is 1.3 km below the shaft collar and 1.5 km below the ground surface, which slopes steeply up away from the shaft in the direction of the stope. The vein had been mined 77% of the 90 m from the 4600 to the 4300 level, leaving a pillar 21 m high at the time of destressing, close to the critical height (*1*). Additionally, the stope was showing fairly high rates and numbers of microseismic events.

The usual indicator of the success of destressing used by mine management is the presence of a significant seismic event on the surface seismograph coincident with destress blasting or before work resumes in the stope (2-4 days). No such seismic event was observed coincident with the destress blast on February 2.

However, within 3 weeks of the February 2 destress, several significant events were detected with the surface seismograph and identified as originating in the 46-99 stope area. Locations for five events subsequent to the destress for which magnitudes could be determined are shown in figure 5. Because of hardware limitations, not all of these events were recorded by the stope digital seismic accelerometer array (described in the next section). In the cases where digital data were not available, locations are from a stope-level automatic system, which identifies arrival times electronically (*7*). Table 1 lists the events shown in figure 5, their magnitudes, seismic energy, amount of damage, and their locations. Especially for the largest events, the locations may not be representative of the site of the largest moment release. (Moment is the product of the shear modulus, the slipped area, and the magnitude of slip.) Within the accuracy of the location method, each location is representative of the event nucleation site.

Table 1.—Destress blast and postdestress seismic events with $M_L \geq 0.6$

Date[1]	Time[2]	M_L	E, J	Damage	Comments
900202	144910	0.4	2.5×10^5	None reported	Destress blast.
900204	035210	1.2	4.0×10^6	Roof fall in stope	None.
900207	034500	2.9	1.4×10^9	5-6 cars muck down	Largest event in mine during 20-month period.
900207	122020	0.9	1.4×10^6	Track uplifted above stope	None.
900215	135421	0.6	5.0×10^5	None reported	Do.
900219	144603	1.2	4.0×10^6	. . do.	Event occurred 25 min after first production blast following destress.

E Energy.
M_L Local magnitude.
[1]Format of this field is yymmdd, where yy = year, mm = month, and dd = day.
[2]Format of this field is hhmmss, where hh = hour, mm = minute, and ss = second.

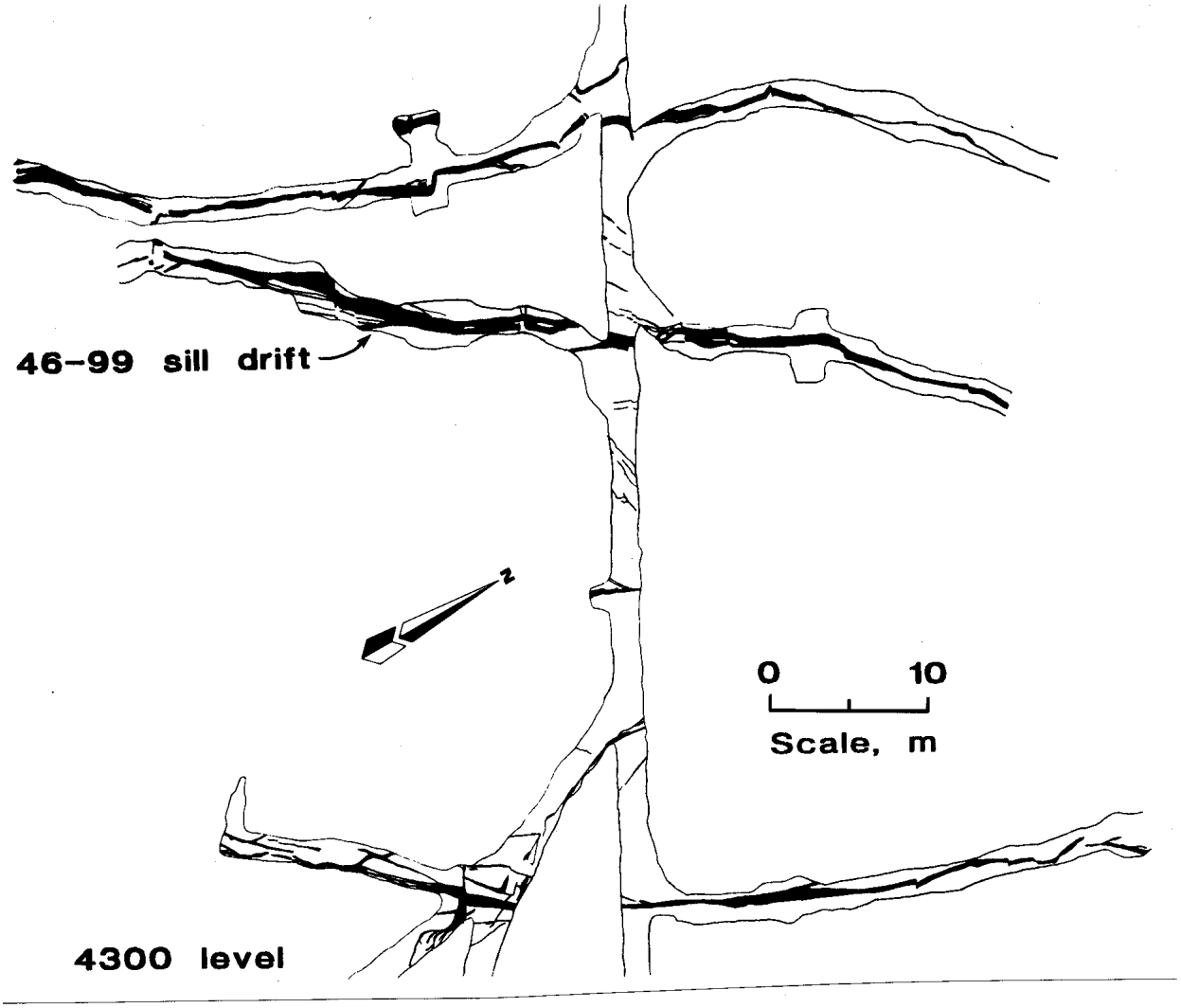

Figure 3.—Plan view map of vein exposures in drifts and crosscuts of 4300 level in vicinity of 46-99 sill drift.

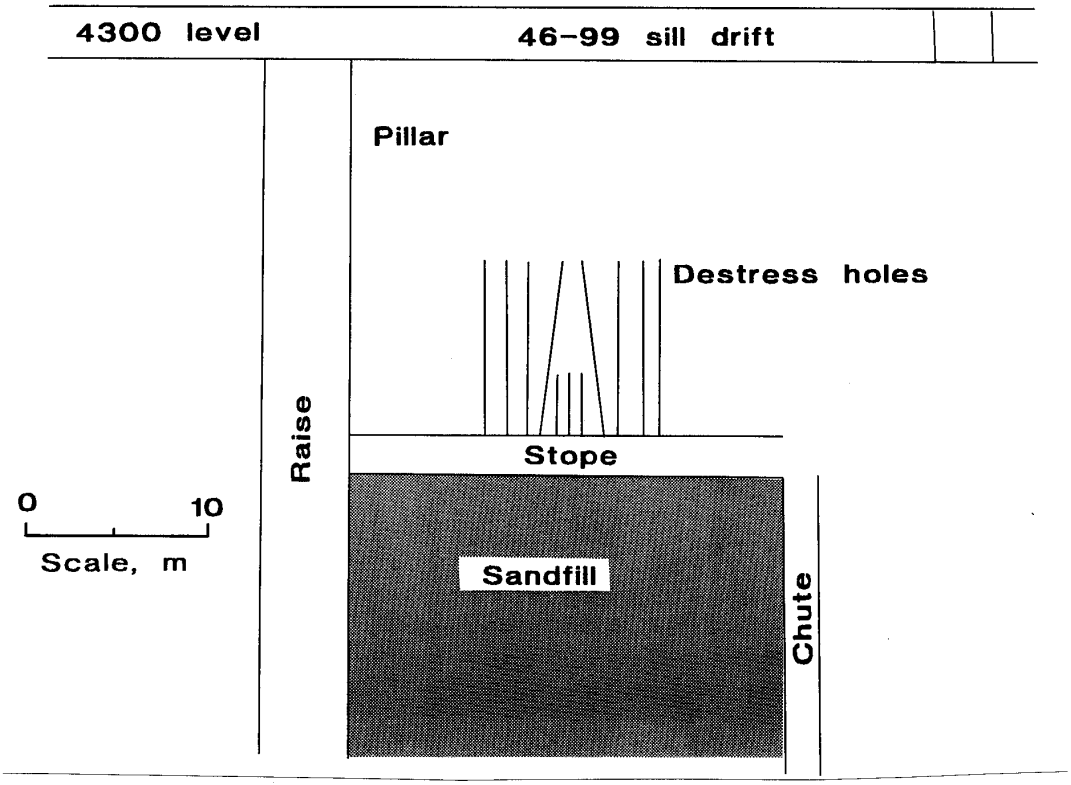

Figure 4.—Schematic vertical section view of 46-99 stope during February 2, 1990, destress blast. Eight 10-m boreholes and three 4-m boreholes were filled with total of 125 kg of explosives for destress.

ACKNOWLEDGMENTS

The authors acknowledge ASARCO Incorporated for their cooperation with the Bureau in providing information, access, and assistance for the data-gathering phase of this research. Clinton Sines, engineering technician, Denver Research Center, provided invaluable on-site expertise and assistance. Louis Estey, geophysicist, Denver Research Center, wrote the three-dimensional rendering and data-fitting software used in data analyses. Robert Simpson, geophysicist, U.S. Geological Survey, Menlo Park, CA, provided the three-dimensional dislocation code.

INSTRUMENTATION

SEISMIC INSTRUMENTATION

Surface Seismometer

The seismic sensor deployed in an adit near the surface is a Teledyne Geotech S-510[3] short-period, vertical-velocity gauge. Its location is 1.3 km vertically above and 0.2 km laterally northwest from the 46-99 stope. The signal is amplified, filtered, and displayed via drum recorder. The gain is adjusted so that microseismic events associated with ordinary production blasting are just visible above the background noise level. Local magnitudes for most located events fall in the range -0.5 to 2.9 (*6*). The largest magnitude event in the mine during a 20-month study period, M_L = 2.9, occurred 5 days after the February 2, 1990, destress blast of the 46-99 stope pillar. Its hypocenter was 110 m from the stope [February 7, 1990, 034500 (hour, minute, second), in figure 5]. (All times in this report are Pacific standard time.)

[3]Reference to specific products does not imply endorsement by the U.S. Bureau of Mines.

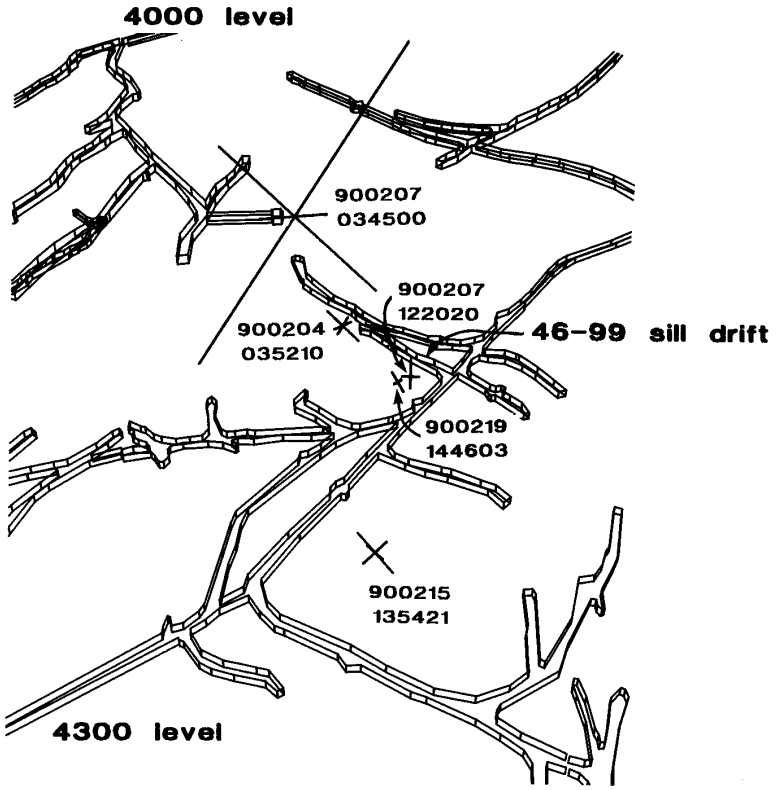

Figure 5.—Oblique perspective view of mine openings and events with $M_L \geq 0.6$ detected by surface seismograph in 46-99 stope area during time period between February 2, 1990, destress and first day of production (February 19) in stope following destress. Event identifiers show date as top six-digit number (year, month, and day) and time (hour, minute, and second) as bottom six-digit number. Lengths of axes are uncertainty for event source location in axis direction. Event with largest location uncertainty (900207, 034500) is outside of most of array. [For scale, mine openings are 3 m (10 ft) high.]

Stope-Level Routine-Monitoring Accelerometer Array

The 46-99 stope is one of eight stopes that are each monitored with a stope-level accelerometer array with a characteristic dimension of approximately 150 m laterally and 180 m vertically. Steblay (*7*) describes the characteristics of this monitoring system. The 46-99 array consists of 16 rib-mounted Wilcoxon 793 M40 accelerometers with 40 V/g sensitivity over 3 to 6,000 Hz. Arrival times of signals are determined by hardware electronic circuitry when a floating threshold is exceeded. These relative times are transmitted to a computer, which calculates and displays locations in near real time for analysis by mine personnel. The arrival times from this system were used in a few cases in which the digital system did not record a particular event of interest.

Digitally Recorded Stope-Level Accelerometer Array

The routine-monitoring stope-level array was augmented by two additional rib-mounted accelerometers and four borehole-mounted, three-component accelerometer packages. The analog signals from these accelerometers were digitally recorded using a 12-bit computer-automated measurement- and control (CAMAC)-based data acquisition system (*8*). Figure 6 shows the locations of the accelerometers in the augmented array. The digitizing rate was 50 kHz or 20 μs between samples. The system provides for on-scale recording of events in the approximate Richter magnitude range -5 to -2. With this setup, significant events within the stope are always clipped (exceed the dynamic range of the digitizers).

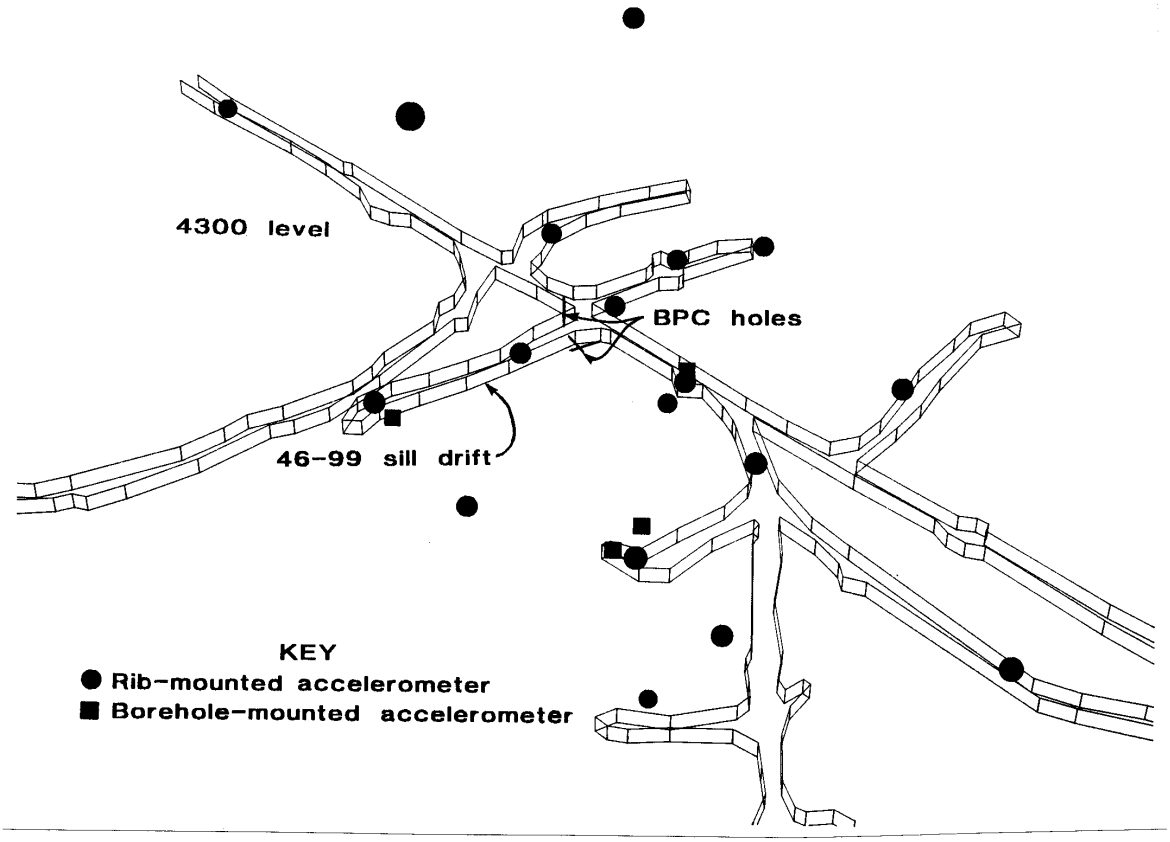

Figure 6.—Oblique perspective view of mine openings, rib- and borehole-mounted accelerometers in 46-99 digitally recorded accelerometer array, and BPC hole array. [For scale, mine openings are 3 m (10 ft) high.]

STRESS-MONITORING INSTRUMENTATION

The Bureau's borehole pressure cell (BPC), described in detail by Haramy (*9*), was used to monitor stress changes caused by destressing and seismic events. The BPC consists of a stainless steel, oblong, pancake-shaped bladder encased in a cylinder of grout, molded to be just under the size of the borehole (60 mm). Cell emplacement includes inserting the package in the borehole and aligning, and pumping the bladder to a preselected setting pressure, typically selected to approximate the overburden pressure (*9*).

Figure 7 shows the position and orientation of the eight BPC's installed at the end of July 1989. Cells were emplaced in three mutually perpendicular 6-m-long boreholes. The geometry of the BPC array was selected based on the observation that the majority of faults trend N. 45° W. and are near vertical. Laboratory observations show that faults tend to form at 30° to 45° to the maximum principal stress direction. If the fault orientation is representative of the present stress field, then BPC's oriented at 45° to the fault will be sensitive to pressure changes in the principal stress orientations. This concept is illustrated in figure 8.

The overburden pressure in the vicinity of the 46-99 stope is estimated at 34 to 37 MPa (from the overburden thickness of 1.5 km and the rock density of 2,400 to 2,600

kg/m³). This area is believed to be under high horizontal tectonic stress. A nominal setting pressure of 35 MPa (5,000 psi) was used with six of the eight cells (1, 2, 3, 4, 6, and 7). In addition, two cells (5 and 8 in figure 7) in redundant orientations to two other cells (6 and 7) were emplaced with a nominal setting pressure of 28 MPa (4,000 psi) as a check on the effect of the absolute setting pressure on cell output.

Prior to February 1990, dial pressure gauge readings were manually recorded. Figure 9 shows the time history of manually recorded cell pressure readings. Digital logging of data began in February 1990, with readings logged for each cell every 10 min. Cell pressures were converted to voltages using Bourns 35 MPa (5,000 psi) pressure transducers (gauges with a larger maximum pressure were not available). Gauge outputs were recorded by the CAMAC system using a 32-channel digital voltmeter module. The pressure transducer installed at cell 2 did not return reliable readings because of electrical problems; therefore, it will not be discussed further.

By the end of January, the absolute pressures for the various cells had diminished, in some cases significantly (cells 5 and 6), below the installation setting pressure. This was partially in response to a rock burst in the vicinity on October 5, 1989. It was expected that the magnitude of pressure changes (due to seismic events, for example) would be affected by the absolute magnitude of pressure in the cell. Data from the cells in redundant orientations did not bear out this expectation, at least for the range of total pressures and pressure changes observed (see "Borehole Pressure Cell Observations" section).

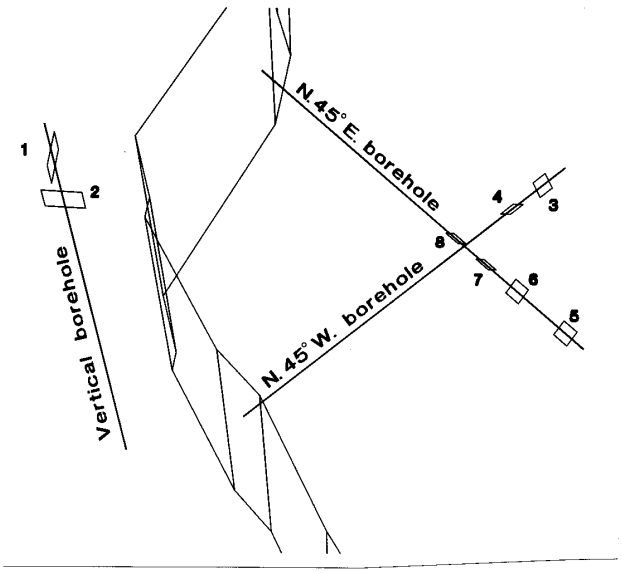

Figure 7.—Oblique perspective view of BPC array geometry, with eight cells (numbered 1-8) mounted in three mutually perpendicular 6-m-long boreholes. Cells 1 and 2, in vertical borehole, have horizontal sensitive axes oriented east-west (cell 1) and north-south (cell 2). Cells 3 and 4 are located in N. 45° W. trending borehole. Their sensitive axes are perpendicular to one another, and both are at 45° to vertical. Cells 5-8 are located in the N. 45° E. borehole. Cells 5 and 6 have duplicate orientations, as do cells 7 and 8. Sensitive axes of cells 5 and 6 are perpendicular to those of cells 7 and 8. Sensitive axes for all four cells in this hole are at 45° to vertical. [For scale, boreholes are 4.6 m (15 ft) long.] (See figure 6 for location of BPC hole array.)

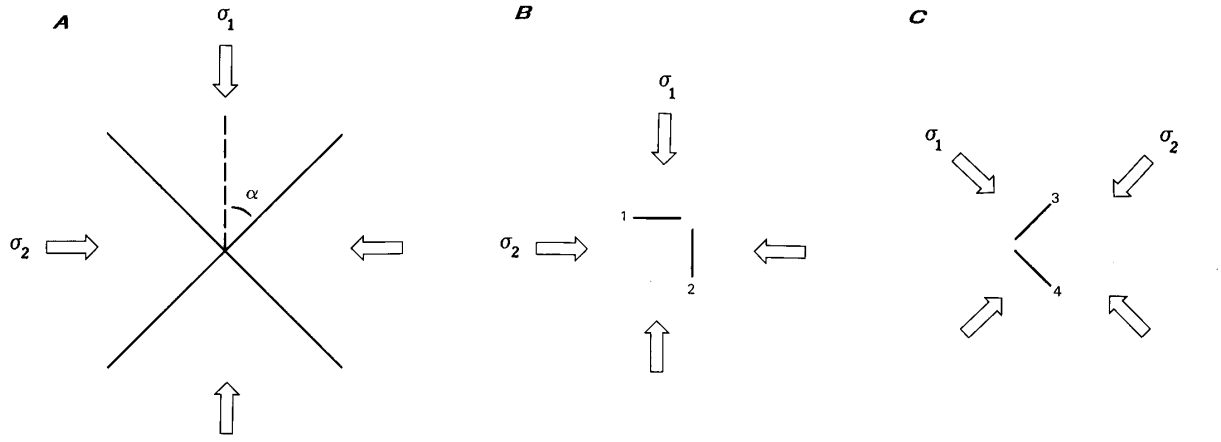

Figure 8.—Selection of cell orientations (numbered 1-4). *A*, Faults typically form at an angle α = 30° to 45° to maximum principal stress (σ_1) direction; *B*, for vertical N. 45° W. faults, cells 1 and 2 are oriented to sense principal stresses that might be responsible for strike-slip motions; *C*, similarly, cells 3 and 4 are oriented to sense principal stresses that might be responsible for dip-slip motion (view looking N. 45° W.). Cells 5-8 are oriented to sense stresses in plane of fault.

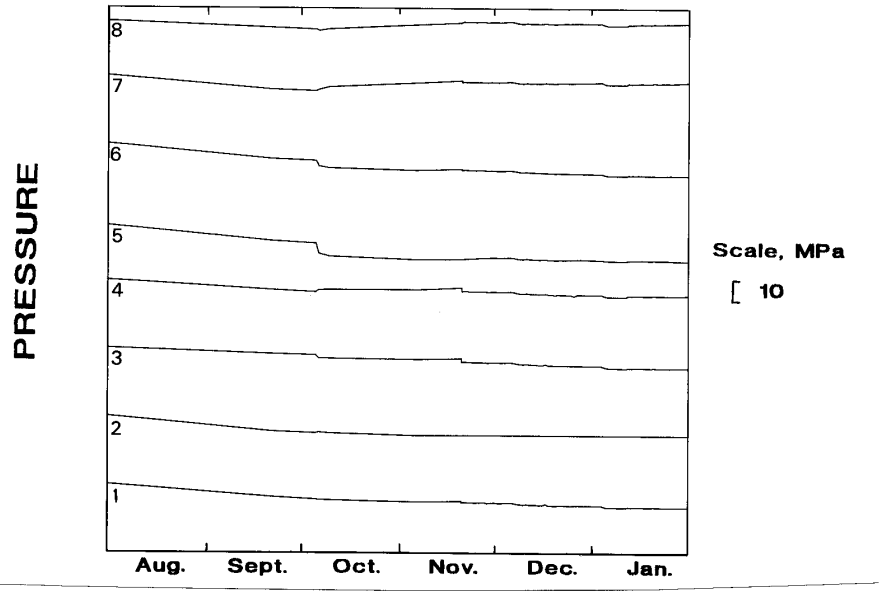

Figure 9.—Time history of pressure recorded manually for BPC array from installation at end of July 1989 through January 1990. An offset on several cells is evident, coinciding with time of October 5, 1989, rock burst, which took place near 46-99 stope. (Curves are labeled with cell numbers; curves are offset for clarity and do not indicate relative or absolute pressure differences among cells.)

SEISMIC EVENTS

Table 1 and figure 5 indicate the significant events that followed the destress of February 2, 1990. The Gutenberg-Richter magnitude-energy scale (*10*) shows that by far the largest energy-release event is the one at 034500 on February 7 (table 1). This event released 350 times the energy of the next largest event. The location of this event coincides with the plane that marks the locus of damaging seismic events occurring in the mine during a 20-month study period discussed above (*5*). Because this event and the event at 122020 later the same day caused damage, these two events are the subject of the analysis that follows.

Noteworthy events that are believed to be related to the two damaging events on February 7 are shown in figures 10 (for the 034500 event) and 11 (for the 122020 event). The five events shown in figure 10 are distinguished from the hundreds that triggered the routine-monitoring system during the 0300 hour because either their energy was sufficient so that they were detected on the surface seismograph, or the energy as monitored by the routine-monitoring system was unusually high. These five events can be enclosed by a sphere 185 m in diameter; this volume is comparable to that expected to be affected by the strain release in the event. The events related to the 122020 event, shown in figure 11, have very similar waveform first-motion polarity-pattern distributions (*11*) to the 122020 event. Since they are in the same place, within the location uncertainty, this is taken as evidence that the mechanism is the same for all these events.

EVENT MECHANISMS

Event focal mechanisms were estimated for the 034500 and 122020 events. The principle and methods for determining focal mechanisms are described in various literature; one report is by Bath (*12*).

Although it is well known that the velocity structure in the vicinity of the mine is strongly heterogeneous (and possibly weakly anisotropic) (*13*), an accurate velocity model is not yet available. In lieu of such a model, a constant velocity of 5.02 km/s was used for both the location of events and for focal mechanism determinations; this value was determined from plots of travel time versus distance for calibration blast tests performed earlier in a nearby and overlapping microseismic array. The inaccuracy of the velocity model means that computed takeoff angles and azimuths are inaccurate by an unknown amount corresponding to the difference between the constant velocity model used and the true velocity structure.

It is only possible to estimate event mechanisms for those events that were recorded by the digital system, since otherwise no first arrival polarity information is retained. Unfortunately, the 034500 event was not recorded by the digital system. To determine a possible fault plane solution for the 034500 event, the foreshock at 030326 (fig. 10), for which digital data were available, was used. This foreshock was located in the same place as the 034500 event, within the location uncertainty. A fault plane solution was also estimated for the damaging event at 122020.

The mechanism for the foreshock to the 034500 event, shown in figure 12, is poorly constrained. The figure shows two possible end members based on one nodal plane (N. 55° W.) that is reasonably consistent with the plane locus of large seismic events occurring throughout the mine identified by Swanson (*5*). Clearly there are many other possible solutions consistent with the limited data. Readings for stations with near-grazing incidence at the accelerometer (±10°) are not shown.

The 122020 event mechanism is inferred from a composite of six events, including the 122020 event. This composite, shown in figure 13, indicates a fairly well-constrained mechanism. The northwest-striking nodal plane is consistent with the N. 45° W. predominant strike of mapped faults in the mine. Given the uncertainty in the velocity structure, and the limitations of the constant velocity model used, it is encouraging to see that this composite can define a solution fairly well.

Figure 14 shows the 034500 and 122020 event mechanisms superimposed on a geologic map of the 4300 level. The trace of the plane defined by the largest seismic events in the mine (*5*) is also shown.

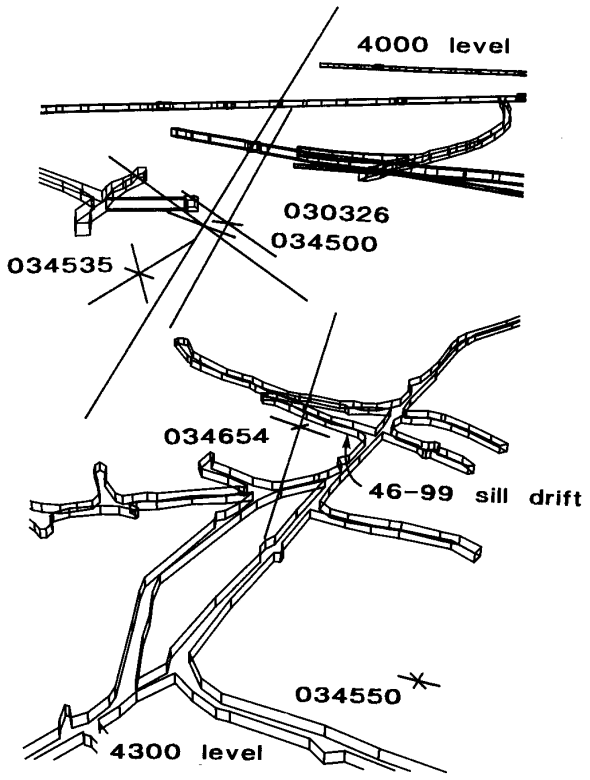

Figure 10.—Oblique perspective view of mine openings and events temporally related to 034500 event. [For scale, mine openings are 3 m (10 ft) high.] (Six-digit numbers refer to hour, minute, and second.)

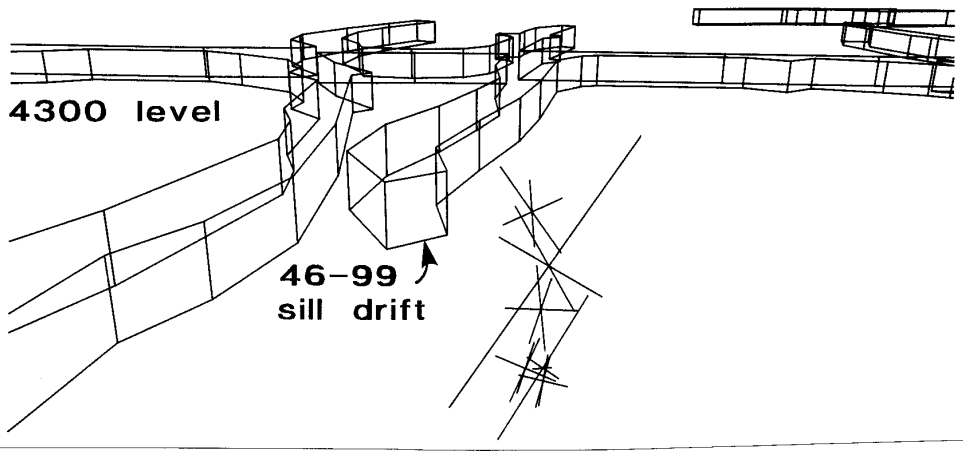

Figure 11.—Oblique perspective view of mine openings and events with similar polarity pattern distributions to 122020 event, indicating same focal mechanism (when events are located in same place). These events were used to generate a composite focal mechanism for 122020 event. [For scale, mine openings are 3 m (10 ft) high.]

The mechanisms shown in figure 14 were used to constrain dislocation models of the damaging events from February 7, fit to observed coseismic BPC pressure changes.

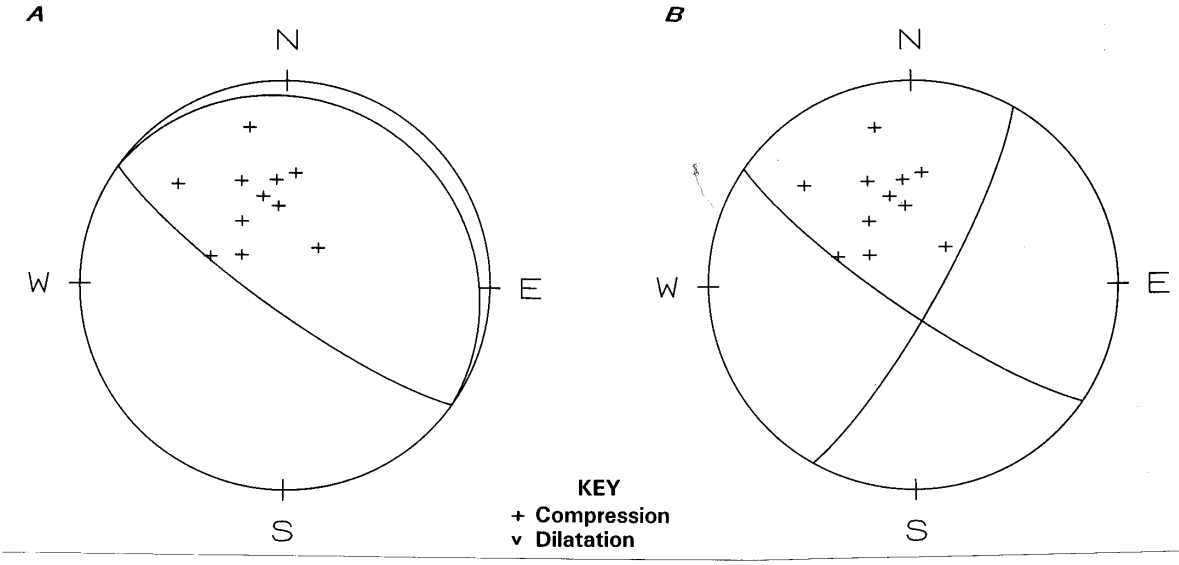

Figure 12.—Two possible fault plane solutions for 030326 foreshock to 034500 event. Readings with angle of incidence >10° not shown. Both solutions have N. 55° W. striking nodal plane, selected to coincide with plane that is apparently the locus of locations of largest events occurring within mine. *A*, Dip-slip mechanism; *B*, strike-slip mechanism.

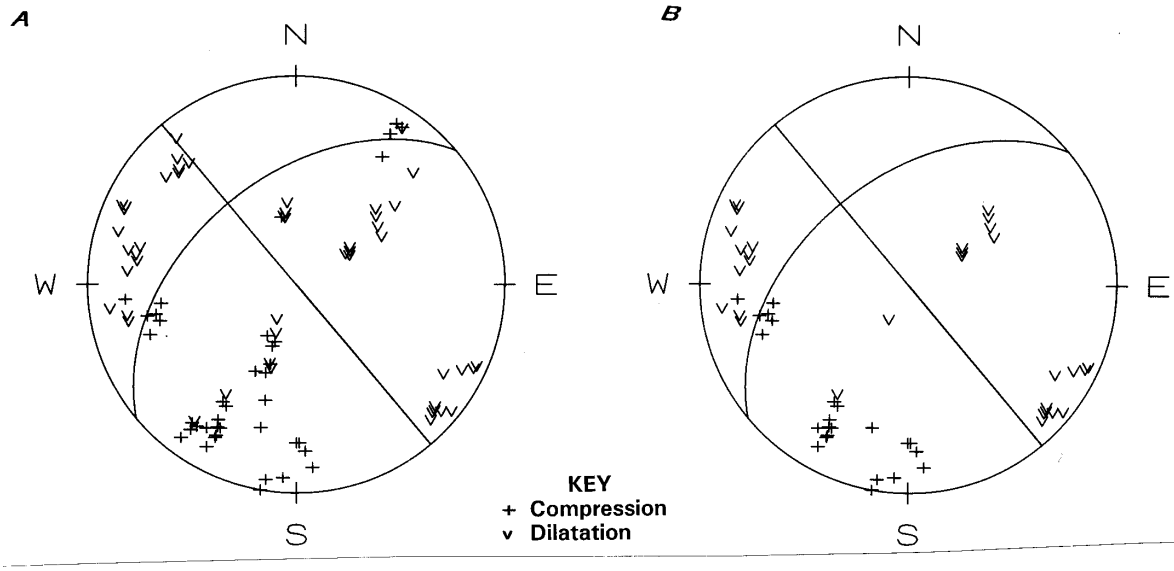

Figure 13.—Composite fault plane solution for 122020 event consisting of readings for that event and the events shown in figure 11. *A*, All readings; *B*, readings with angle of incidence at accelerometer >10°.

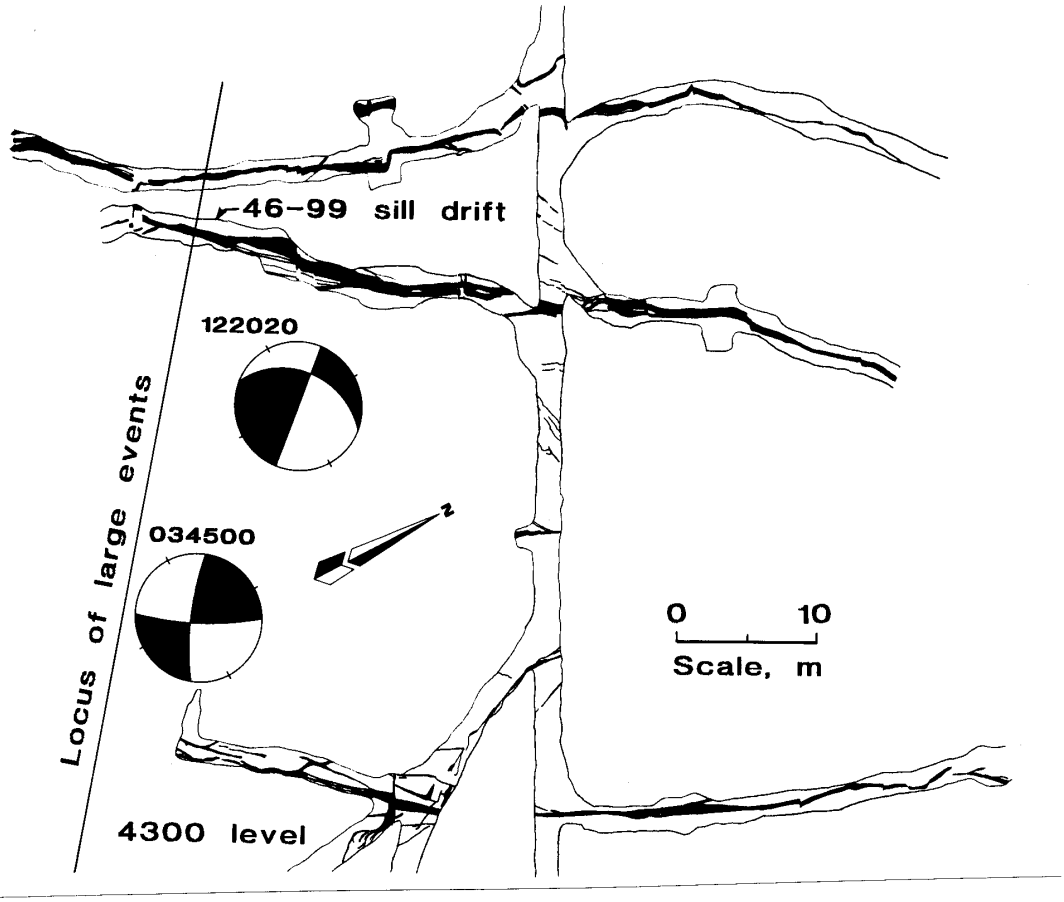

Figure 14.—Fault plane solutions for 034500 and 122020 events with plan view map of vein exposures and drifts and crosscuts of 4300 level in vicinity of 46-99 sill drift.

BOREHOLE PRESSURE CELL OBSERVATIONS

Figure 15 shows the time history of BPC measurements from the beginning of February through February 8, 1990. There is a certain amount of "cultural" noise that occurs when shift crews are working (probably electric motor noise). This is evident in comparison with times such as the weekend from February 3 to 4, when the signals were significantly quieter. This noise limits the resolution of offsets caused by specific seismic events.

Figure 16 shows the BPC measurements for February 7. Changes coinciding in time with the observed events, within the 10-min resolution of the measurements, are observed for both of the damaging event sequences (034500 and 122020). The earlier offset is correlated with the 034500 event rather than the 034654 event (fig. 10) because of the large seismic energy of the 034500 event (table 1). All of the pressure changes observed are positive for the 034500 event. For the 122020 event, a decrease in pressure was observed for cells 5 and 6, which have identical orientations. The magnitude of pressure changes for both events on all the cells is a few hundred kilopascals maximum. Although the 034500 event had a much larger magnitude, the 122020 event was much closer to the BPC array; hence, the resultant observed pressure offsets are of the same magnitude for both events. Figure 17 shows a similar time period around the destress blast on February 2. From a comparison of figures 16 and 17, the seismic events (fig. 16) caused a far larger coincident change in stress than did the destress blast itself.

Comparison of offsets on duplicate cells 5 and 6 and cells 7 and 8 (fig. 16) indicate that the magnitudes of the measured pressure offsets are not significantly affected by the total absolute pressure. [The total pressure for cell 6

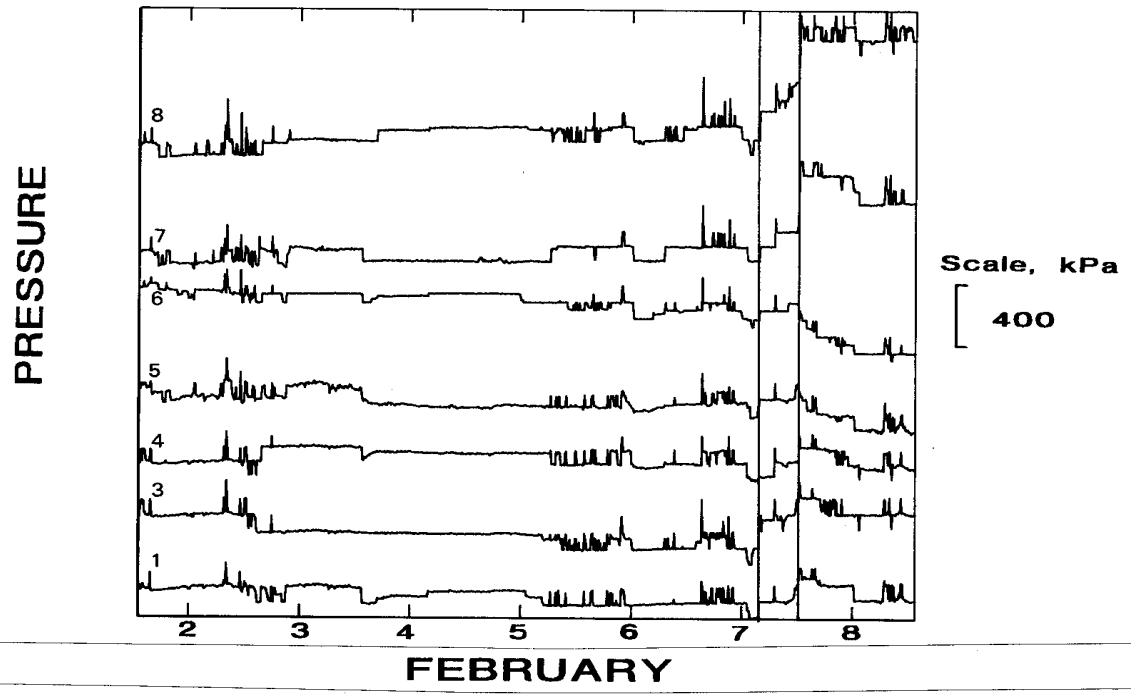

Figure 15.—Digitally logged BPC data for February 1-9, 1990. Period of less noisy data on February 3 and 4 is the weekend, when minimal crews were working. (Curves are labeled with cell numbers; curves are offset for clarity and do not indicate relative or absolute pressure differences among cells. Times corresponding to 034500 and 122020 events on February 7 are shown as vertical lines.)

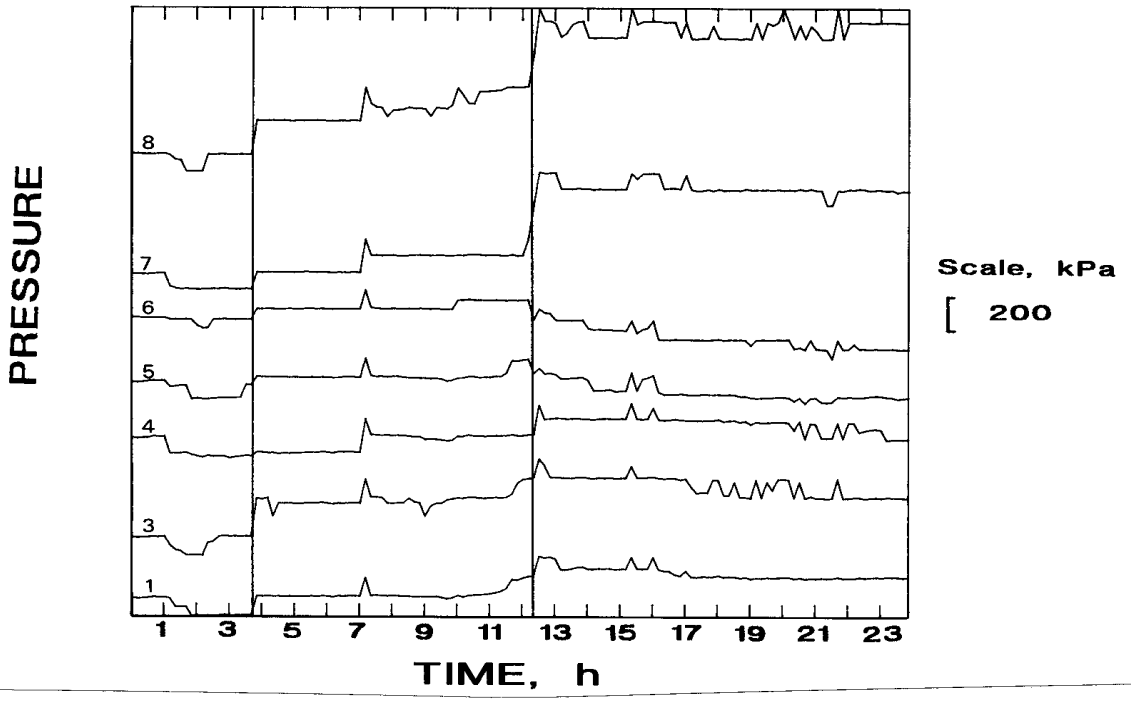

Figure 16.—BPC data for February 7, 1990. (Curves are labeled with cell numbers; curves are offset for clarity and do not indicate relative or absolute pressure differences among cells. Times corresponding to 034500 and 122020 events are shown as vertical lines.)

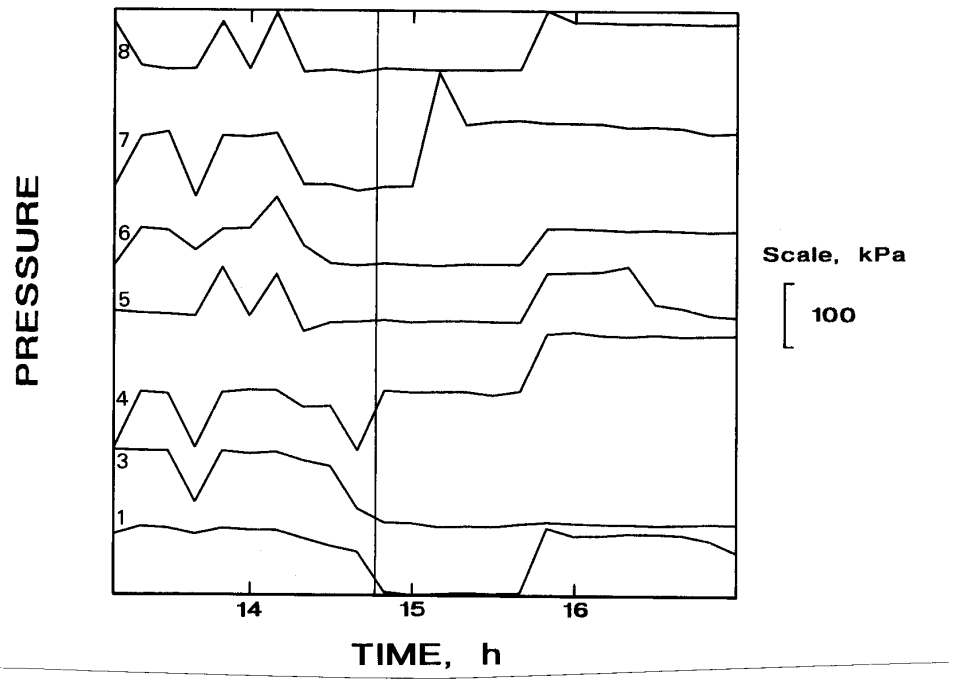

Figure 17.—BPC data for February 2, 1990. (Curves are labeled with cell numbers; curves are offset for clarity and do not indicate relative or absolute pressure differences among cells. Time corresponding to destress is shown as vertical line.)

(19 MPa) is about twice that of cell 5 (10 MPa); the total pressure for cell 7 (32 MPa) is about 15% higher than that of cell 8 (27 MPa).] The observed offsets due to the February 7 and other events are not significantly different for these duplicate oriented cells in spite of the differences in total pressure.

DISLOCATION MODELS OF FAULT OFFSET

By using dislocation models of seismic sources, static changes in elastic field values (after minus before) caused by fault slip can be computed; for an example, see reference 14. These models are based on analytic expressions for the elastic fields developed by a rectangular dislocation (*15*). Computations in this report were done with a FORTRAN program described by Erickson (*16*). Such models were used to find the amount of fault slip necessary to fit the observed pressure offsets at the BPC array. The available seismic measurements (event location and fault plane solution) were used to constrain the location, size, orientation, and sense of slip for the dislocation models. Dislocation models were also used to evaluate the effect of the 034500 event on the fault plane site of the 122020 event.

FITS TO BOREHOLE PRESSURE CELL DATA

The focal mechanisms determined above were used to define fault planes for each of the 034500 and 122020 events. Magnitudes for these two events were obtained using the coda duration (of seismic signal after first arrival) fit by Swanson (*6*). Slip areas were estimated using magnitude-area relations (*17*). Fault plane solution information was used to constrain the possible sense of slip for the 034500 event, but not the relative amounts of strike slip and dip slip, since these were not constrained by the available polarity data. For the 122020 event, the fault plane solution was used to constrain the relative amounts and sense of strike and dip slip. The magnitude of slip was then determined by the best fit to the measured BPC

offsets. Figure 18 shows the measured BPC records for the 034500 (*A*) and 122020 (*B*) events along with the best fit offsets (least squares) using dislocation slip models. For the redundantly oriented BPC's, only cells 6 and 8 were used in the fits since their total pressures were closest to the average total pressure for the other cells of the array. The 034500 event was modeled as a vertical-rectangular dislocation 297 m on a side, centered at the located event. The model for this event allowed the relative amounts of strike slip and dip slip to be obtained from the fit. The best fit at 95% confidence has 1.09 (±1.18) mm left-lateral strike slip and 1.6 (±0.99) mm northeast-downward dip slip. The large uncertainty in fit can be attributed to measurement error and to inadequacy of the homogeneous elastic media of the dislocation model for describing the actual response of the fractured rock mass.

The 122020 event (fig. 18*B*) was modeled as a vertical-rectangular dislocation, 28 m on a side, centered at the location for that event. The dislocation is oriented N. 40° W., consistent with the vertical nodal plane of the mechanism. (The other nodal plane would require right-lateral strike slip motion only. Such motion results in BPC offsets in the opposite sense from those observed for all but cells 5 and 6.) The orientation and relative amounts of northeast-downward dip slip and left-lateral strike slip were determined by the composite focal mechanism as shown in figure 13. The total amount of slip that best fits the offsets at 95% confidence was 0.45 (±0.55) mm.

There are several possible reasons for the large uncertainties in the fit for this event:

1. Measurement error.
2. The homogeneous elastic model may not adequately represent the complex stope geometry in the vicinity of this event.
3. There may have been a localized inelastic response of the rock mass at the BPC array because of its close proximity to the 122020 event.
4. The cells are very close to the fault, and their response may be strongly influenced by the details of the fault geometry. This affects the offsets computed by dislocation modeling as well, because in this case the cell array turns out to be 15 m from the top edge of the dislocation and 20 m from the center, in an area of rapidly changing stress field. Since the position of the dislocation center with respect to the hypocenter is not well constrained, a better fit might be obtained by adjustment of this parameter. Similarly, there is an uncertainty in the size and shape of the dislocation patch, where a rectangular patch is used as a matter of convenience. The role of uncertainty in the patch geometry is probably dominated by edge effects, i.e., exactly where the patch boundaries fall relative to the BPC array.
5. Deviation from the assumed planar slip surface may play a role. For example, the orientation of the fault may have shifted away from the fault plane solution after slip began.
6. Cells 5 through 8 are less smooth in their behavior than the others for this event: During the previous 10-min interval, they show changes in pressure of about the same magnitude as the observed changes during the 10-min interval that encompasses the event.

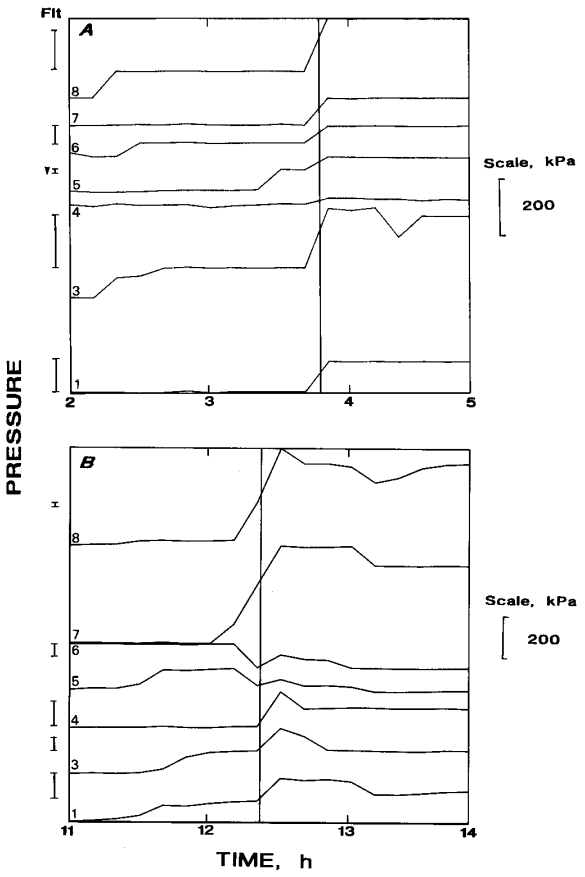

Figure 18.—Fits of measured pressure changes on BPC array computed using dislocation sources. (Curves are labeled with cell numbers; curves are offset for clarity and do not indicate relative or absolute pressure differences among cells. Fitted offsets are shown to left of each curve used in fit.) *A*, Fit for 034500 event. Amount of slip was 1.1 mm of left-lateral strike slip and 1.6 mm of northeast-downward dip slip; *B*, fit for 122020 event. Relative amounts of strike slip and dip slip were constrained by fault plane solution (see figure 13).

EVENT INTERACTION

The dislocation parameters that fit the BPC data for the 034500 event were used to calculate the induced changes in stress field components in the vicinity of the 122020 event. The results are used to determine if the stress changes produced by the 034500 event inhibit or enhance the prospects for slip of the type observed for the 122020 event. Figure 19 shows the shear and normal stresses on the 122020 fault induced by the dislocation on the 034500 fault (see "Fits to Borehole Pressure Cell Data" section). This dislocation results in a decrease in normal stress of somewhat less than 0.2 MPa across the 122020 fault. This would enhance the possibility for slip in any direction on this plane. This dislocation also induced an increase in shear stress favoring southwest-downward dip slip of 0.4 MPa (maximum) and a decrease in shear stress favoring left-lateral strike slip of 0.3 MPa (maximum). The composite focal mechanism for the 122020 event shows a combination of left-lateral strike slip and southwest-downward dip slip. Ignoring the preexisting tectonic and mining-induced stresses acting on the 122020 fault, the potential for the observed southwest-downward dip slip was enhanced by the 034500 dislocation, while the potential for the observed left-lateral strike slip motion was inhibited by the 034500 dislocation. Two components of the induced stress field enhanced the possibility for the observed slip, suggesting that the 034500 event was important in promoting the occurrence of the 122020 event later that day.

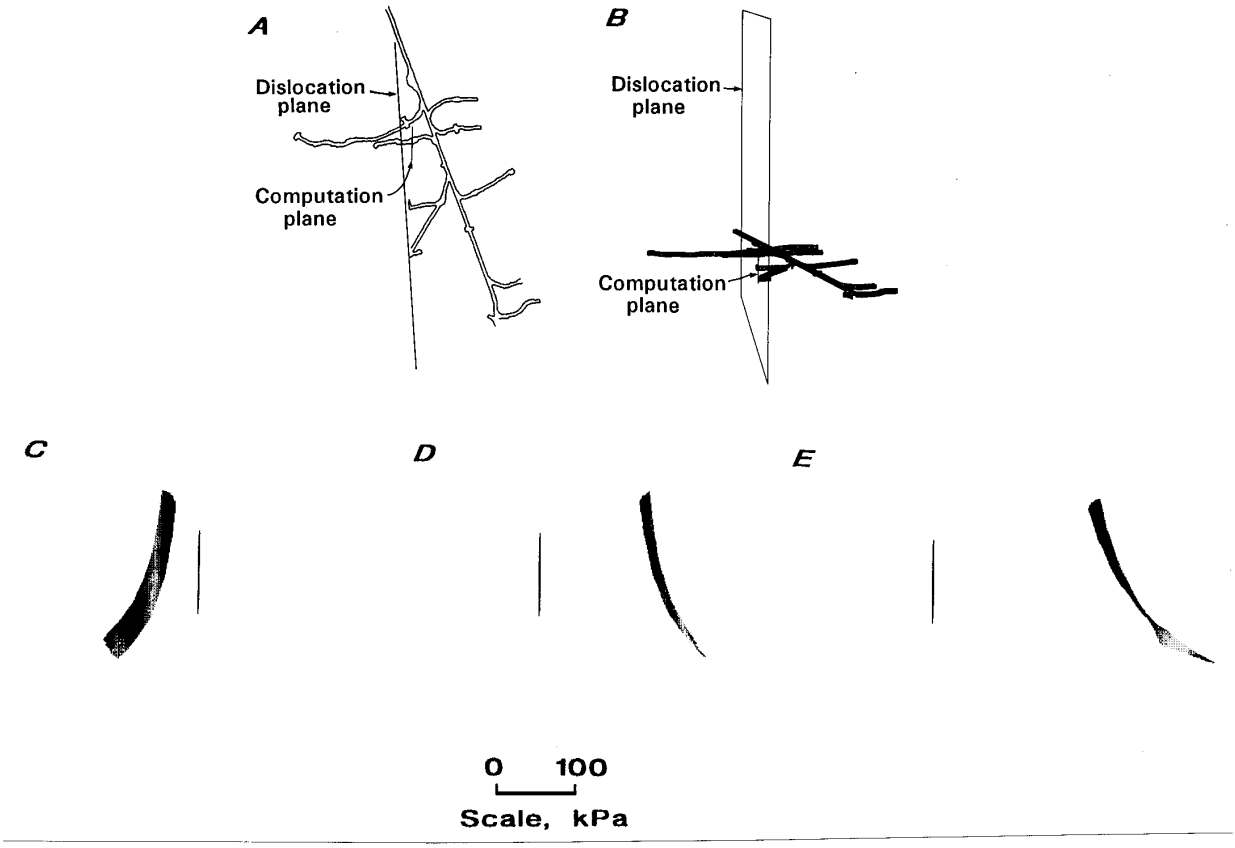

Figure 19.—Stress field on 28- by 28-m fault plane for 122020 event, induced by dislocation slip on 297- by 297-m fault plane of 034500 event. *A*, Plan view of 4300 level showing plane of dislocation and plane of computation; *B*, oblique perspective view looking parallel to plane of computation; *C*, induced normal stress. Distance in direction perpendicular to computation plane (vertical line) of each point of gray-tone surface is proportional to induced stress. Since surface is completely to left of computation plane, induced stress is all tensile; *D*, induced strike slip shear stress. Induced stresses are in the sense to favor right-lateral strike slip; *E*, induced dip slip shear stress. Induced stresses are in the sense to favor southwest-downward dip slip.

DISCUSSION

The broader purpose of this work is to show how quantitative observation and analysis of destressing attempts can lead to a better understanding of the process and to the ability to design better destress methods. For the February 2, 1990, destress, there is BPC and seismological information available for analysis. The following sections present a review of the seismological data for evidence of a connection between the destress and subsequent events. Possible ways to improve destress effectiveness are also discussed.

MEASURED PRESSURE CHANGES DURING DESTRESS

Figure 17 shows that pressure changes due to the destress, as monitored at the BPC array, were no more than the noise level, which was at about 100 kPa at that time. Blake (*1*) computed the stress field in a pillar before and after destressing using a two-dimensional, finite-element model. A hydrostatic stress of 52 MPa was applied to the model. Maximum stresses in the pillar as a function of pillar height were computed, along with the contours of the stress field. For the pillar height at the time of the February 2 destress, the maximum stress in the pillar expected from Blake's model is 165 MPa. In the model, after destressing, the maximum stress in the pillar was reduced to about 60 MPa, assuming that the destress reduced the Young's modulus of the pillar by more than 80% because of fracturing. No such dramatic reduction in stress was observed on the BPC array at the time of the February 2 destress. This array samples ground within 5 m of the pillar and 25 m of the center of the destress round. Unless the BPC array was shielded somehow from the effects of the destress, the measurements suggest that the destress reduced Young's modulus (induced fracturing) by an amount far smaller than the 80% assumed by Blake. Such shielding is possible, given the fractured nature of the ground and the ability of fractures to act as stress discontinuities.

RELATIONSHIP OF DESTRESS TO SUBSEQUENT SEISMIC EVENTS

There is evidence both for and against the notion that the destress triggered the subsequent seismic events. This evidence is summarized as follows.

Evidence Supporting Connection Between Destress and Subsequent Events

The evidence supporting a connection is that the destress may have marked the onset of a flurry of seismic activity unmatched in the previous year in this stope. The activity following the destress is intense and unusual (fig. 1). Eight significant events occurred in the vicinity of the 46-99 stope from January 1989 through February 1, 1990. Seven events occurred beginning with the destress on February 2 through February 19, 1990. Seven additional events occurred from March 1990 through the end of the survey period in October 1990. Similar activity did not follow the other two destresses of the stope in December 1989 and June 1990. It cannot be ruled out that the flurry of activity may be coincidentally associated with the destress. Generally, mine management expects a large seismic event coincident with an effective destress blast. However, destresses are always scheduled on a Friday's last shift so that the possibility of delayed events or large "aftershocks" happening during a working shift is reduced. The first significant event following the destress was a small one that occurred 37 h later; the largest event of the sequence took place 4½ days after the destress.

Evidence Against Connection Between Destress and Subsequent Events

There are four main lines of evidence against a connection between the destress and subsequent events:

1. The time delay that occurred between the destress and subsequent events is significant since no large event occurred at the time of the destress, assuming that the relationship between the flurry of activity in February 1990 discussed above was coincidental.
2. The magnitude of the pressure change observed with BPC's at the time of the destress was negligible, and perhaps not enough of a change to induce a flurry of seismic activity.
3. If a stress discontinuity is invoked to explain the lack of observed pressure changes at the time of the destress blast, an explanation must be made as to why the February 7 events resulted in observable pressure changes when the same (assumed) stress discontinuity should shield the array from effects of these events.
4. By using the measured stress changes on the BPC array from the destress to estimate stress change at the site of the 034500 event hypocenter, assuming a homogeneous elastic medium, magnitudes are yielded on the order of a few kilopascals. This magnitude of stress change would be unlikely to trigger the 034500 event. However, it is more likely that the destress triggered the February 4 event (table 1), which in turn may have triggered the 034500 event on February 7.

IMPROVING DESTRESS EFFECTIVENESS

The destressing method of drilling holes into pillars and blasting has been used for over 20 years in the Coeur d'Alene district. Effort is rarely expended in determining whether existing information can help determine whether the destressing will be effective. With knowledge of the state of stress and the principles of fracture mechanics, it is possible to make educated judgments about whether a particular destressing operation is capable of accomplishing either (1) inducing strain energy release through a coincident seismic event, or (2) softening the remaining pillar rock so that strain energy cannot be stored.

State of Stress Estimates

A stress province map of the continental United States was recently published (*18*). Stress provinces are subregions of the continent that possess similar principal stress directions and relative magnitudes. The stress provinces are formed in response to tectonic processes. Stress data used to establish these provinces include earthquake focal mechanisms, borehole breakouts, in situ stress-relief measurements, hydraulic fracturing, and other stress indicators. The map in reference 18 shows a question mark in the region surrounding northwestern Montana and the northern Idaho Panhandle. The question mark is present not for a lack of stress measurements, but because of inconsistencies in the available data (*19*). Inconsistencies may occur in at least two ways. First, in a stress field that has equal horizontal components, a preferred orientation of directional indicators of stress is not expected. Second, the stress measurements in this region, most of which are stress-relief measurements in Coeur d'Alene mines, may be influenced by stress field heterogeneity induced by mining. Some studies specifically acknowledge this influence. In addition, overcoring stress measurements generally receive the lowest quality rating for use in determining regional tectonic stress (*18*) because many measurements are not presented with evidence of their consistency over suitable distances.

It is easy to understand how individual point measurements of stress made in extensively fractured and faulted ground (fig. 2) may not be representative of regional stress, particularly when measurements are made near high-stress gradients. The Bureau is examining methods to measure principal stresses in fractured and faulted ground by inversion of focal mechanism parameters obtained for groups of distributed microseismic events. Such analyses provide data useful for planning and evaluating destressing techniques, circumventing the complications of making conventional point measurements of stress in inelastic and nonhomogeneous ground.

State of Stress and Destress Strategies

Knowledge of the approximate principal stress directions is essential to design effective destressing strategies. This knowledge is particularly important when relying upon the release of stress by blast-induced cracks; principal stress directions strongly influence crack propagation directions and thus determine the manner in which stresses are rearranged. With a measure of the local (on the scale of a stope) principal stress directions, one may devise a destress strategy based on the actual local conditions that takes advantage of these conditions. The stress field of interest is not necessarily the regional stress field because not only do the workings perturb this stress field, but stoping areas are often in a stress shadow or in an area of stress amplification because of other nearby heterogeneities, particularly mined-out veins, which may or may not be backfilled. In the case of the Galena Mine at the present stage of development, most of the veins are close enough together and of sufficient size for stress interaction to occur. While knowledge of the stress field applied on the scale of the entire mine is certainly beneficial, it is not sufficient for engineering stress control measures in individual, closely spaced stopes.

In the present study, the principal stress directions acting in the pillar were estimated from borehole breakouts that formed when the vertical destress blast holes were drilled. Borehole breakouts, or stress-induced elongation of boreholes, form in a direction perpendicular to the maximum principal compressive stress (*20-21*). In all but one of the destress holes, breakouts were oriented parallel to the strike of the vein, indicating a maximum principal stress component, resolved in the horizontal plane, that was perpendicular to the strike of the pillar. The exception to this trend was a borehole separated from the others by an intervening fault. Its breakout was perpendicular to the others, suggesting that at the time the holes were drilled, the fault surface provided a discontinuity in stress. This observation is an example of the need for multiple consistent stress measurements over a representative distance for high-quality stress determinations. With the principal stress directions in hand, one can estimate the influence of the stress field on blast-induced crack formation and propagation in the pillar. It is well known from fracture mechanics that tensile fractures tend to propagate parallel to the direction of maximum principal compressive stress. This is also a very stable crack geometry in that, once the dynamic crack propagation phase ceases, the driving force for crack extension increases only with further increases in applied load (*22*). It is also known that propagation of cracks from a region of low stiffness (for example, the ore vein) into a region with higher stiffness (for example, the quartzite country rock)

is not favored. (This neglects the effects of pervasive fracturing on the stiffness of either the ore vein or the country rock.) There is a tendency to deflect away from the stiff region back into the low-stiffness material. Thus, any cracks that initially extend in the direction of the maximum principal stress may deflect away from high-stiffness country rock. Once deflected, such a crack is no longer optimized for releasing stored elastic strain energy because of the maximum principal stress.

To make effective use of principal stress data and the basic principles of fracture mechanics, the objective of destressing must be taken into account. If it is to release, in a controlled fashion, the stored elastic strain energy that is capable of being released in the largest expected rock burst (i.e., without triggering a large rock burst), then the destress blast pattern should be large enough and of the appropriate layout. This may be impractical, in which case alternative methods should be considered. What is the volume of rock that releases strain energy during the largest (M_L ~ 3) rock bursts at the Galena Mine? Swanson (*6*), using several different approaches to estimating this volume, suggests that a magnitude 2.9 rock burst may be driven by elastic strain energy release from a volume as large as 2.4×10^7 m^3 or a sphere of ~300 m diameter. This characteristic source dimension is not unique, however, and will depend upon, for a given event magnitude (or seismic moment), the stress or strain drop associated with the release mechanism (i.e., the lower the stress drop, the larger the volume). The volume of stress release associated with a magnitude +3 event with a small to modest stress drop will not likely be released controllably by any amount of destress blast drillholes in a single pillar. Destress blasting may, however, influence the initiation of such an event; to do this in a planned way would require a sophisticated understanding of the current stress and stability state of the structure and how to modify these. The February 7, 1990, 034500 M_L ~ 2.9 event produced significantly elevated microseismic activity in stopes encompassing a volume of 2×10^7 m^3. The stored energy associated with a smaller magnitude but potentially very destructive event with high stress drop centered on a single stope may conceivably be released controllably by destress blasting in that particular stope.

If the objective is to trigger a large seismic event, then the destress strategy should be designed to optimize triggering; this is not necessarily consistent with softening the pillar. Other methods such as water infusion may be more suited to accomplishing this objective. At the present time it is not possible to be specific, without being unduly speculative, about which method should be used because this requires a firm understanding of the mechanisms of rock bursting. While the state of understanding is growing rapidly in this area and the tools highlighted in this report are being used to help characterize rock burst mechanisms, current understanding is not sufficiently developed at this point to make detailed recommendations for changes in destress strategies. It is quite apparent that an understanding of rock burst mechanisms is the first step required for developing triggering or avoidance methods in the most effective and safe manner.

CONCLUSIONS

Examples of the use of new analysis techniques, such as focal mechanisms and dislocation modeling, for quantitatively describing mining-induced ground deformation have been presented. These techniques, which are still under development and adaptation for use in the mining environment, are being evaluated by the Bureau to determine if they can provide the information needed to evaluate existing stress control methods and to design new methods.

Seismic observations and measurements of changes in ground stress were made in conjunction with a destress of the 46-99 stope of the Galena Mine. Similar observations were made of seismic events that occurred during the 2½ weeks following the destress. Two of the seismic events during this period caused damage to the mine. These two events were studied in depth to identify their relationship to one another and the destress. Focal mechanisms for the damaging seismic events were used as constraints for dislocation models computed to fit the observed pressure offsets on an array of BPC's. These computations showed that the larger damaging seismic event was probably an important factor in promoting the occurrence of the smaller damaging event later the same day.

Given the observed small stress change due to the destress on February 2, 1990, and the evidence from the state of stress and fracture mechanics considerations, some recommendations about destressing can be made. First, adequate knowledge of the existing local stress field is necessary for designing appropriate hole patterns for blast destressing. While in situ stress can be accurately measured at individual points using, for example, overcoring techniques, this is probably impractical for the majority of situations where destressing will be attempted. Further, it does not provide adequate three-dimensional local stress field information. Knowledge of the far-field stresses from available tectonic and regional seismic data, combined with numerical modeling of the effect of mining in the area to be destressed, may be a more practical approach. Any additional knowledge from borehole breakouts to analyses of in-mine or stope-level seismic and microseismic mechanisms is desirable. Second, blast hole patterns for

the most effective crack growth pattern must be designed with consideration of the existing stress field and the available access. Third, any means of monitoring the response of the rock mass to the destress, such as ground pressure or microseismic monitoring, is highly desirable so that destress effectiveness can be evaluated.

REFERENCES

1. Blake, W. Destressing Test at the Galena Mine, Wallace, Idaho. Soc. Min. Eng., AIME Trans., v. 252, 1972, pp. 294-299.

2. Leighton, F. W. A Case History of a Major Rock Burst. BuMines RI 8701, 1982, 14 pp.

3. Cook, N. G. W., E. Hoek, J. P. G. Pretorius, W. O. Ortlepp, and M. D. G. Salamon. Rock Mechanics Applied to the Study of Rockbursts. S. Afr. Inst. Min. and Metall. J., v. 66, 1966, pp. 436-528.

4. Hobbs, S. W., A. B. Griggs, R. E. Wallace, and A. B. Campbell. Geology of the Coeur d'Alene District, Shoshone County, Idaho. U.S. Geol. Surv. Prof. Pap. 478, 1965, 139 pp.

5. Swanson, P. L., and C. D. Sines. Repetitive Seismicity (M ~ 2-3) and Rock Bursting Along a Plane Parallel to Known Faulting in the Coeur d'Alene District, ID. EOS Trans. Am. Geophys. Union, v. 71, 1990, p. 1453.

6. ____. Characteristics of Mining-Induced Seismicity and Rock Bursting in a Deep Hard-Rock Mine. BuMines RI 9393, 1991, 12 pp.

7. Steblay, B. J., B. T. Brady, and T. Swendseid. Innovative Microseismic Monitoring System. Paper in Proceedings of the 2nd International Symposium on Rockbursts and Seismicity in Mines (Minneapolis, MN, 1988). Balkema, 1990, pp. 259-262.

8. Boler, F. M., and P. L. Swanson. Computer-Automated Measurement- and Control-Based Workstation for Microseismic and Acoustic Emission Research. BuMines IC 9262, 1990, 9 pp.

9. Haramy, K. Y., and R. O. Kneisley. Hydraulic Borehole Pressure Cells: Equipment, Technique, and Theories. BuMines IC 9294, 1991, 26 pp.

10. Gutenberg, B., and C. Richter. Seismicity of the Earth. Princeton Univ. Press, 1949, 273 pp.

11. Billington, S., F. M. Boler, P. L. Swanson, and L. H. Estey. P-Wave Polarity Patterns From Mining Induced Seismicity in a Hard-Rock Mine. Paper in Proceedings of the 31st Symposium on Rock Mechanics. CO Sch. Mines, Golden, CO, 1990, pp. 931-938.

12. Bath, M. Introduction to Seismology. Birkhaeuser (Basel), 2d ed., 1979, 428 pp.

13. Estey, L. H., P. L. Swanson, F. M. Boler, and S. Billington. Microseismic Source Locations: A Test of Faith. Paper in Proceedings of the 31st Symposium on Rock Mechanics. CO Sch. Mines, Golden, CO, 1990, pp. 939-946.

14. Chinnery, M. A. The Stress Changes That Accompany Strike Slip Faulting. Bull. Seismol. Soc. Am., v. 53, 1963, pp. 921-932.

15. Mansinha, L., and D. E. Smyllie. The Displacement Field of Inclined Faults. Bull. Seismol. Soc. Am., v. 61, 1971, pp. 1433-1440.

16. Erickson, L. L. A Three-Dimensional Dislocation Program With Application to Faulting in the Earth. M.S. Thesis, Stanford Univ., Stanford, CA, 1986, 167 pp.

17. Utsu, T., and A. Seki. A Relation Between the Area of After-Shock Region and the Energy of Main Shock. J. Seismol. Soc. Japan (Zisin), v. 7, 1955, pp. 233-240 (in Japanese).

18. Zoback, M. L., and M. D. Zoback. Tectonic Stress Field of the Continental United States. Paper in Geophysical Framework of the Continental United States. Geol. Soc. Am. Mem. 172, 1989, pp. 523-539.

19. Zoback, M. L. (U.S. Geological Survey). Private communication, 1991; available from P. L. Swanson, BuMines, Denver Research Center, Denver, CO.

20. Gough, D. I., and J. S. Bell. Stress Orientation From Borehole Wall Fractures With Examples for Colorado, East Texas, and Northern Canada. Can. J. Earth Sci., v. 19, 1982, pp. 1358-1370.

21. Haimson, B. C., and C. G. Herrick. Borehole Breakouts—A New Tool for Estimating In-Situ Stress? Paper in Proceedings of the International Symposium on Rock Stress and Rock Stress Measurements (Stockholm, Sept. 1-3, 1986). Centek, 1986, pp. 271-280.

22. Rooke, D. P., and D. J. Cartwright. Compendium of Stress Intensity Factors. Hillingdon Press, London, 1976, 330 pp.